Spatio-Temporal Dynamics in Collective Frog Choruses Examined by Mathematical Modeling and Field Observations

Ikkyu Aihara[1], Takeshi Mizumoto[2], Takuma Otsuka[2], Hiromitsu Awano[2], Kohei Nagira[2], Hiroshi G. Okuno[2] & Kazuyuki Aihara[3]

[1]Brain Science Institute, RIKEN, Saitama 351-0198, Japan, [2]Graduate School of Informatics, Kyoto University, Kyoto 606-8501, Japan, [3]Institute of Industrial Science, The University of Tokyo, Tokyo 153-8505, Japan.

This paper reports theoretical and experimental studies on spatio-temporal dynamics in the choruses of male Japanese tree frogs. First, we theoretically model their calling times and positions as a system of coupled mobile oscillators. Numerical simulation of the model as well as calculation of the order parameters show that the spatio-temporal dynamics exhibits bistability between two-cluster antisynchronization and wavy antisynchronization, by assuming that the frogs are attracted to the edge of a simple circular breeding site. Second, we change the shape of the breeding site from the circle to rectangles including a straight line, and evaluate the stability of two-cluster and wavy antisynchronization. Numerical simulation shows that two-cluster antisynchronization is more frequently observed than wavy antisynchronization. Finally, we recorded frog choruses at an actual paddy field using our sound-imaging method. Analysis of the video demonstrated a consistent result with the aforementioned simulation: namely, two-cluster antisynchronization was more frequently realized.

C horuses of male frogs can be detected in various places, e.g., the streams in rain forests and the edges of ponds[1–3]. The spatial distribution of calling frogs is significantly diverse depending on species and their habitats. Japanese tree frogs (*Hyla japonica*) are one of the commonest frog species in Japan[4]. Choruses of male Japanese tree frogs are audible at night mainly along edges of paddy fields, which contain rich water suitable for cultivation of rice, between early spring and late summer. Laboratory experiments have revealed various types of their synchronized calling behavior, e.g., antisynchronization of two individual frogs[5], and 1:2 antisynchronization and tri-phase synchronization of three individual frogs[6]. In choruses at a paddy field, male Japanese tree frogs dynamically change their calling times and positions based on acoustic interactions with other individuals. The spatio-temporal dynamics in such interactive choruses can be mathematically understood as a system of coupled oscillators[5–8]. Our motivation in this study is to investigate the spatio-temporal dynamics of their choruses in natural habitats.

Spatio-temporal dynamics in coupled-oscillator systems, collective or not, has been studied both experimentally and theoretically. Experimental studies revealed various types of the spatio-temporal structures in the real world. For instance, the Belousov-Zhabotinsky reaction generated rich examples of pattern formation such as target patterns and spiral waves[8,9]; experiments on colliding microtubules yielded self-organized structures of large-scale vortex lattices[10]. Furthermore, theoretical studies elucidated plausible nonlinear mechanisms generating such spatio-temporal dynamics. For example, a phase oscillator model provided a valuable tool describing synchronization phenomena in coupled-oscillator systems[8]; the phase oscillator model was then extended to include a system consisting of mobile oscillators[11–13]. We previously demonstrated that the synchronized behavior of male Japanese tree frogs observed in laboratory experiments could be qualitatively explained as a system of coupled but not mobile oscillators[5–7].

On the other hand, the collective behavior of animals, e.g., flashing of fireflies[9] and chirping of crickets[1], has been attracting a great deal of attention in the light of biology as well as many other disciplines. These animals dynamically change their positions and also interact with each other by using various signals such as bioluminescence and chirping. Consequently, we can expect to observe various spatio-temporal structures in their posi-
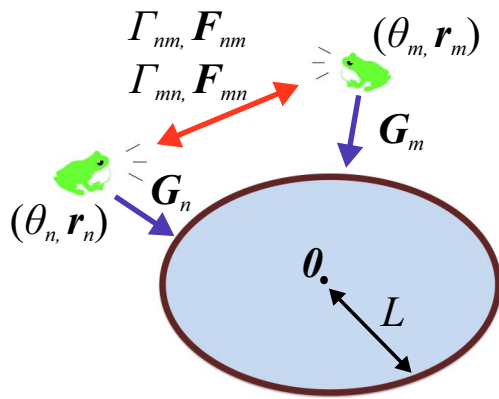
Figure 1 | A schematic diagram describing our mathematical model of equations (5) and (6) that are mentioned in Methods. The calling times and position of the nth frog are modeled by using the calling phase θ_n and the spatial position $\boldsymbol{r}_n$, respectively. The nth and mth frogs mutually interact according to the functions Γ_{nm}, Γ_{mn}, $\boldsymbol{F}_{nm}$, and $\boldsymbol{F}_{mn}$. The function $\boldsymbol{G}_n$ is used to explain our field observations that male Japanese tree frogs aggregate along the edges of paddy fields. The geometric shape of the field is first assumed to be a circle with the radius L and the origin $\boldsymbol{0}$, for simplicity. This diagram was drawn by I.A.

tions and signals. However, field research of such structures in animal behavior has been restricted because of the difficulties faced in carrying out such research, e.g., in finding where many individuals exist and how they are spatially distributed. Studying the collective behavior of Japanese tree frogs via field research and mathematical modeling could contribute to further understanding of collective animal behavior, and could also aid in extending the framework of the phase oscillator model.

Results

Numerical simulation of spatio-temporal dynamics in collective frog choruses at a circular field. We model the spatio-temporal dynamics inherent in the calling times and positions of male Japanese tree frogs by using equations (5)–(9) that are mentioned in Methods. Based on this model, we theoretically examine organized structures in their choruses at a paddy field. Note that the geometric shape of a paddy field is first assumed to be a circle in this model, for simplicity (Fig. 1). The parameter values of the model are then fixed on the basis of laboratory experiments and field observations. Laboratory experiments have revealed that an isolated male Japanese tree

frog calls about 4 times per second[5], so that the intrinsic angular velocity ω_n in equation (5) is fixed as $\omega_n = 8\pi$ rad/s for all the individual frogs. Furthermore, in our field observations, the perimeter of all the edges of a paddy field was typically more than 100 m, and more than about 20 individual frogs simultaneously called in one paddy field. Therefore, the radius of the paddy field L and the total number of the male frogs N are fixed as $L = 20$ m and $N = 20$, for simplicity. However, since the parameter K_{nm} in equations (7) and (8) is difficult to be estimated from laboratory experiments or field observations, K_{nm} is fixed to be the unit value as $K_{nm} = 1$, for simplicity.

Figures 2 and 3 show the results of numerical simulation, which are obtained by assuming different initial conditions but the same parameter values $\omega_n = 8\pi$ rad/s, $L = 20$ m, $N = 20$, and $K_{nm} = 1$. Frogs are indexed from 1 to N along the edge of the circular field in the counterclockwise direction (Fig. 2A). Our simulation demonstrates that two kinds of spatio-temporal dynamics are bistable depending on the initial conditions (Figs. 2 and 3). The first dynamical structure is shown in Figure 2A and B; whereas the male frogs are positioned along the edge of the field at the same interval (Fig. 2A), each neighboring pair of male frogs synchronize in anti-phase, forming two clusters (Fig. 2B). The second structure is shown in Figure 3A and B; whereas the male frogs are positioned along the edge of the field as well (Fig. 3A), each neighboring pair of male frogs synchronize in almost anti-phase with a spatial phase shift (Fig. 3B); consequently, a wavy state is realized in each cluster, which can be described as $\theta_n - \theta_{n+1} = \pi + \dfrac{2k\pi}{N}$ by using a nonzero integer k describing the wave number of this state. We name the spatio-temporal dynamics in Figure 2 as *two-cluster antisynchronization*, and that in Figure 3 as *wavy antisynchronization*.

To detect occurrences of two-cluster and wavy antisynchronization, we introduce the following order parameters $R_{cluster}$ and R_{wavy} as the extensions of the order parameter for in-phase synchronization[8], i.e., $R_{in} = \left| \sum_{n=1}^{N} \exp(i\theta_n) \right| \Big/ N$:

$$R_{cluster} = \frac{1}{N} \left| \sum_{n=1}^{N} \exp(i2\theta_n) \right|, \qquad (1)$$

$$R_{wavy} = \frac{1}{N} \left| \sum_{n=1}^{N} \exp\left[i2\left(\theta_n + \frac{2nk\pi}{N} \right) \right] \right|. \qquad (2)$$

Figures 2C and 3C show the time series data of $R_{cluster}$, R_{wavy}, and R_{in}. When two-cluster antisynchronization is realized as shown in
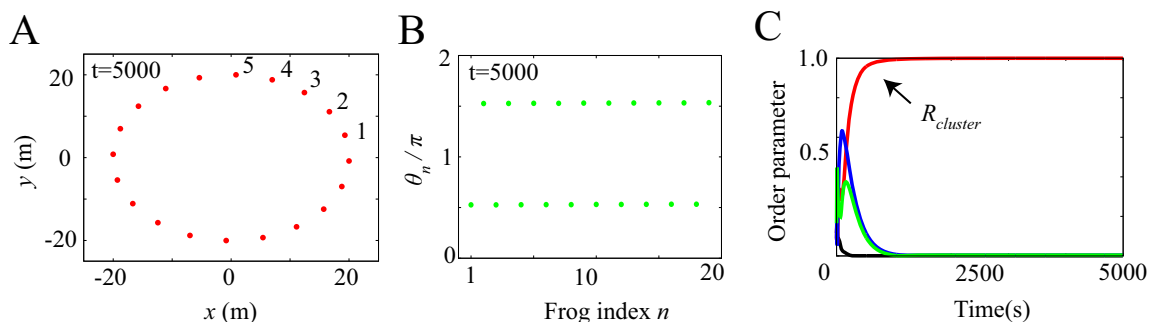

Figure 2 | Two-cluster antisynchronization obtained from our numerical simulation on the assumption of $\omega_n = 8\pi$ rad/s, $L = 20$ m, $N = 20$, and $K_{nm} = 1$ in equations (5)–(9). (A) Spatial structure in a frog chorus. Frogs are positioned along the edge of the circular field at the same interval. An index n is attached to each frog along the edge of the field in the counterclockwise direction. (B) Two-cluster antisynchronization in a frog chorus. The horizontal axis represents the frog index n, and the vertical axis represents θ_n at $t = 5000$. Each pair of neighboring frogs synchronize in anti-phase π, and then two-cluster antisynchronization is realized. (C) Time series data of the order parameters $R_{cluster}$ and R_{wavy} defined in equations (1) and (2), and $R_{in} = \left| \sum_{n=1}^{N} \exp(i\theta_n) \right| \Big/ N$[8]. Red, blue, green, and black lines represent the time series data of $R_{cluster}$, R_{wavy} for $k = 1$ and $k = -1$, and R_{in}, respectively. When two-cluster antisynchronization is realized as shown in Figure 2B, only $R_{cluster}$ takes a high value around 1.
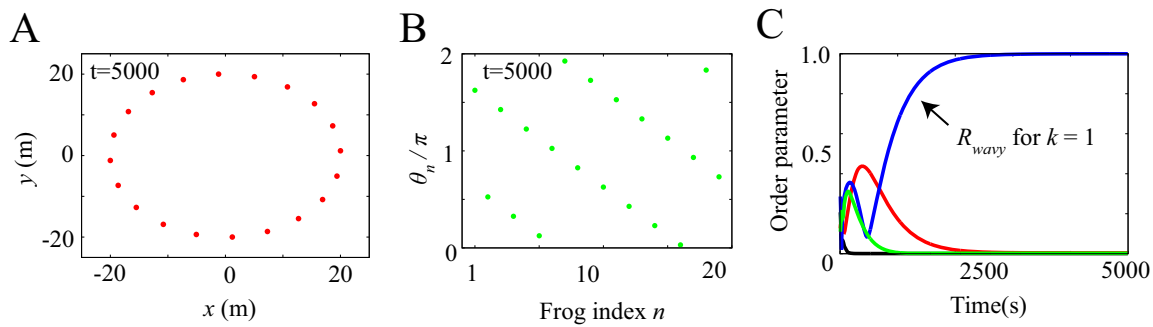
Figure 3 | Wavy antisynchronization obtained from our numerical simulation with the same parameter values as those in Figure 2 but with a different initial condition. (A) Spatial structure in a frog chorus. Frogs are positioned along the edge of the circular field at the same interval. (B) Wavy antisynchronization in a frog chorus. Neighboring frogs synchronize in almost anti-phase π, and then a wavy state is generated in each cluster. (C) Time series data of the order parameters $R_{cluster}$, R_{wavy} and R_{in}. Red, blue, green, and black lines represent the time series data of $R_{cluster}$, R_{wavy} for $k = 1$ and $k = -1$, and R_{in}, respectively. When wavy antisynchronization is realized as shown in Figure 3B, only R_{wavy} for $k = 1$ takes a high value around 1.

Figure 2B, only $R_{cluster}$ takes a high value around 1 (Fig. 2C). In contrast, when wavy antisynchronization is realized as shown in Figure 3B, only R_{wavy} for $k = 1$ reaches a high value around 1 (Fig. 3C). Thus, the order parameters $R_{cluster}$ and R_{wavy} can be used to discriminate between two-cluster antisynchronization and wavy antisynchronization. In addition, we perform linear stability analysis by assuming circular distribution of the calling frogs, and show that both two-cluster antisynchronization and wavy antisynchronization are asymptotically stable (see Supplementary information). Note that the same parameter values are assumed for the linear stability analysis, i.e., $\omega_n = 8\pi$ rad/s, $L = 20$ m, $N = 20$, and $K_{nm} = 1$.

Numerical simulation of the stability of two-cluster antisynchronization and wavy antisynchronization at a rectangular field. The usual geometric shape of a paddy field is not a circle but a rectangle in Japan. In this section, the stability of two-cluster antisynchronization and wavy antisynchronization is analyzed by replicating the shape of an actual paddy field in our model.

We describe the shape of a rectangular paddy field by using two parameters L_x and L_y, which represent the length and width of the

field, respectively (Fig. 4A). In addition, the summation of L_x and L_y is constrained as $L_x + L_y = 60$ m, for consistency with the perimeter of the circular field shown in Figures 2A and 3A. Then, $G_n(r_n)$ in equation (6) is defined as follows:

$$G_n(r_n) = r_n^* - r_n, \tag{3}$$

where r_n^* represents the vector from the origin 0 to the point on the edges that is nearest to the position of the nth frog r_n, as shown in Figure 4A. We use the term $G_n(r_n)$ in equation (3), which changes its sign across the boundary condition $r_n = r_n^*$, to explain the attraction of the male frogs towards the edges of the field.

Figure 4B shows the results of numerical simulation based on the assumption of $\omega_n = 8\pi$ rad/s, $N = 20$, $K_{nm} = 1$, and $L_x + L_y = 60$ m in the present mathematical model of equations (3) and (5)–(8). In this simulation, the parameters L_x and L_y are varied with an interval of 2 m in the ranges $30 \leq L_x \leq 60$ and $0 \leq L_y \leq 30$ under the constraint $L_x + L_y = 60$. For each parameter set of L_x and L_y, occurrences of two-cluster antisynchronization and wavy antisynchronization are calculated for 500 runs of the simulation with different initial conditions: namely, if only $R_{cluster}$ is
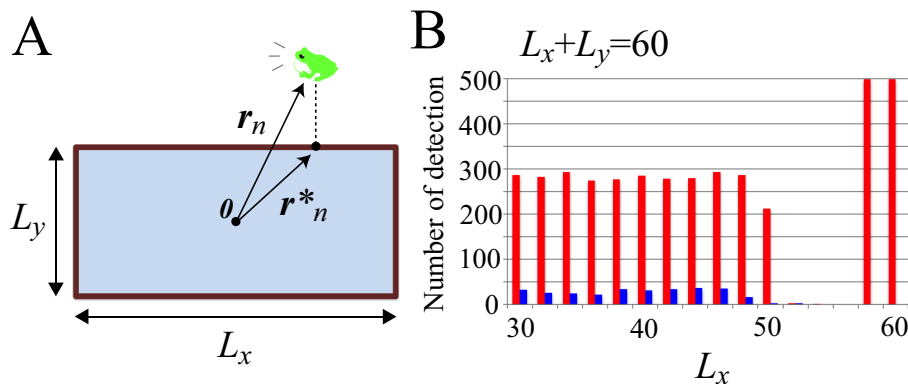

Figure 4 | Numerical simulation on the stability of two-cluster antisynchronization and wavy antisynchronization. The geometric shape of a field is assumed to be a rectangle, so as to replicate the shape of an actual paddy field in Japan. Parameters in equations (3) and (5)–(8) are fixed as $\omega_n = 8\pi$ rad/s, $N = 20$, $K_{nm} = 1$, and $L_x + L_y = 60$ m. (A) A schematic diagram describing the mathematical model. The two parameters L_x and L_y represent the length and width of the field, and r_n^* represents the vector from the origin 0, or the center of the rectangle, to the point on the edges that is nearest to the position of the nth frog r_n. The nth frog is attracted to r_n^*, according to $G_n(r_n)$ described by equation (3). In this simulation, L_x and L_y are varied with an interval of 2 m in the ranges of $30 \leq L_x \leq 60$ and $0 \leq L_y \leq 30$ under the constraint $L_x + L_y = 60$, and occurrences of two-cluster antisynchronization and wavy antisynchronization are calculated for 500 runs of the simulation with different initial conditions at each parameter set: namely, if only $R_{cluster}$ is more than 0.9 at $t = 30000$, the dynamics is considered as two-cluster antisynchronization; if only R_{wavy} is more than 0.9 for one of $k = -4, -3, -2, -1, 1, 2, 3$, and 4 at $t = 30000$, the dynamics is considered as wavy antisynchronization. (B) Results of the numerical simulation on the stability of two-cluster and wavy antisynchronization. Red bars represent the numbers of detection of two-cluster antisynchronization, and blue bars represent those of wavy antisynchronization among 500 runs of the simulation. Two-cluster antisynchronization is more frequently observed than wavy antisynchronization, except for the cases of $(L_x, L_y) = (52, 8)$, $(54, 6)$ and $(56, 4)$. The diagram of Figure 4A was drawn by I.A.
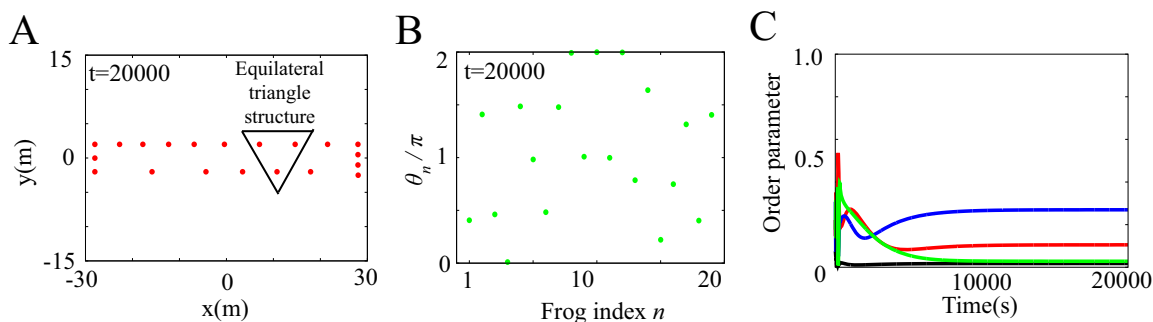
Figure 5 | Spatio-temporal dynamics in a frog chorus obtained from numerical simulation with $\omega_n = 8\pi$, $N = 20$, $K_{nm} = 1$, **and** $(L_x, L_y) = (56, 4)$ **in equations (3) and (5)–(8).** (A) Spatial structure in a frog chorus. Almost equilaterally triangular patterns are generated in many of neighboring frog trios at $t = 20000$, because of the narrow and long geometric shape of the rectangular field characterized by $(L_x, L_y) = (56, 4)$. (B) Disordered phase dynamics in a frog chorus. The horizontal axis represents the frog index n, and the vertical axis represents θ_n at $t = 20000$. A self-organized structure such as two-cluster or wavy antisynchronization is not realized. (C) Time series data of the order parameters, $R_{cluster}$, R_{wavy}, and R_{in}. Red, blue, green, and black lines represent the time series data of $R_{cluster}$, R_{wavy} for $k = 1$ and $k = -1$, and R_{in}, respectively. All the order parameters take considerably less values than 1.

more than 0.9 at $t = 30000$, the dynamics is considered as two-cluster antisynchronization; if only R_{wavy} is more than 0.9 for one of $k = -4, -3, -2, -1, 1, 2, 3$, and 4 at $t = 30000$, the dynamics is considered as wavy antisynchronization. As shown in Figure 4B, two-cluster antisynchronization is more frequently observed than wavy antisynchronization, except for the cases of $(L_x, L_y) = (52, 8)$, $(54, 6)$, and $(56, 4)$.

When $(L_x, L_y) = (52, 8)$, $(54, 6)$, and $(56, 4)$, both two-cluster antisynchronization and wavy antisynchronization are not or very rarely detected (Fig. 4B). Why does such instability occur at these parameter values? Figure 5A and B represents an example of the spatio-temporal dynamics at $(L_x, L_y) = (56, 4)$. As shown in Figure 5A, almost equilaterally triangular patterns are realized in many frog trios because of the narrow and long geometric shape of the rectangular field characterized by $(L_x, L_y) = (56, 4)$. Since the coupling strength of $\Gamma_{nm}(\theta_m - \theta_n, r_m - r_n)$ in equation (7) depends on the distance between frogs, such equilateral-triangle structures cause the frog trios to interact with almost the same strength. Moreover, $\Gamma_{nm}(\theta_m - \theta_n, r_m - r_n)$ in equation (7) is assumed to be a sinusoidal function. It has been theoretically shown that almost the same coupling strength with the sinusoidal function, e.g., $d\theta_n/dt = \omega_n - \sum_{m=1, m \neq n}^{3} K_{nm} \sin(\theta_m - \theta_n)$ with $n = 1, 2, 3$, $\omega_n = \omega$, and $K_{12} = K_{13} \simeq K_{23}$, can strongly frustrate the calling behavior of three frogs[7]. We speculate that such frustration is the source of the instability of two-cluster and wavy antisynchronization at $(L_x, L_y) = (52, 8)$, $(54, 6)$, and $(56, 4)$. In fact, a snapshot of the phases at $t = 20000$ does not show any organized structure such as the two-cluster and wavy antisynchronization (Fig. 5B), and all the order parameters $R_{cluster}$, R_{wavy} and R_{in} take considerably less values than 1 (Fig. 5C).

Thus, our numerical simulation of the present mathematical model suggests that the two-cluster antisynchronization of the male frogs can be more frequently observed than wavy antisynchronization at a rectangular paddy field.

Field research on collective choruses of male Japanese tree frogs. Figure 7A shows the time series data of the light pattern of sound-imaging devices[14] deployed at an actual paddy field (see Methods and Fig. 6), capturing the chorus structures of male Japanese tree frogs. The colored plots represent the light intensity of each device, which has been calculated by subtracting the average light intensity of each device that can slightly vary depending on its tuning[14]; an index is attached to each device from one end of the edge, which is closer to the camera, to the other end (Fig. 6C). The device nearest to each calling frog was estimated every 15 sec, by analyzing the summation of the light intensity of the deployed devices: namely, if the summation at one device exhibited a local peak and exceeded a threshold, the device was determined to be nearest to one calling frog. Through this analysis, the threshold was set as 3×29.97 fps (frames per second) $\times 15$ sec. To estimate the calling times of each frog, the light pattern of the device nearest to each calling frog was then analyzed: namely, when the light pattern of the device exceeded a threshold, the corresponding times were detected as the calling times of the frog (see supplemental materials of the reference 6). In
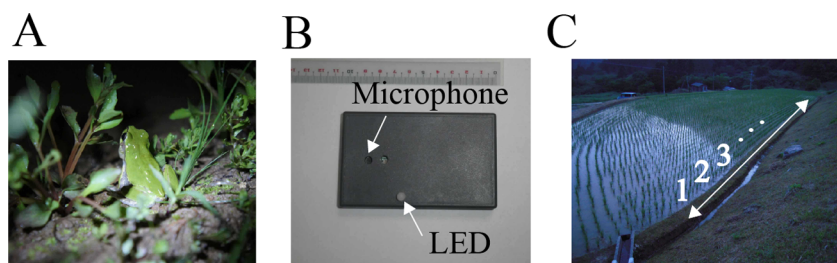

Figure 6 | Field research on frog choruses, by using our sound-imaging method[14]. (A) A photograph of a male Japanese tree frog (*Hyla japonica*). (B) A photograph of our sound-imaging device *Firefly*. The *Firefly* unit consists of a microphone and a light emitting diode (LED) that is illuminated when capturing nearby sounds[14]. (C) A photograph of a paddy field in Japan. Along one edge of this paddy field, we deployed 85 or 86 sound-imaging devices at intervals of 40 cm. As shown here, an index was attached to each device from one end of the edge, which was closer to the camera, to the other end. The spatio-temporal light pattern of these devices was recorded by a video camera. Note that the lights of some devices were not detected, when those devices were deployed far from the camera and were not illuminated by frog calls. We carefully checked all the data, and confirmed that the lights of at least 40 devices close to the camera were stably captured even when those were not strongly illuminated by frog calls. Hence, we used the light patterns of 40 devices close to the camera for data analysis of all the observations. These photographs were taken by I.A. and H.G.O.
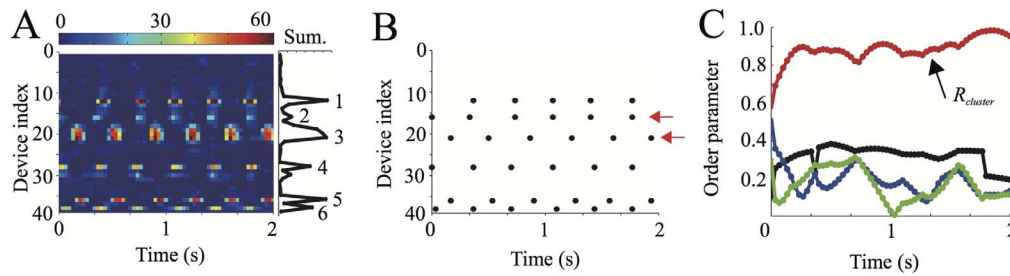
Figure 7 | Spatio-temporal structure in an actual frog chorus obtained by our field research on 15th June in 2011. (A) A light pattern of the sound-imaging devices deployed at the paddy field. While the horizontal and vertical axes represent the time and device index, the colored plots represent the light intensities of the devices[14]. An index was placed on each device from one end of the edge, which was closer to the camera, to the other end. The attached right panel shows the summation of light intensity of each device. This data set represents the calls of 6 frogs numbered from 1 to 6.
(B) Calling times and positions of male Japanese tree frogs. Each black dot represents the calling times and positions of the 6 frogs. We observed that some pairs of these frogs called synchronously. For instance, the 2nd and 3rd frogs stably synchronized in almost anti-phase π (see the two red arrows).
(C) Time series data of the order parameters, $R_{cluster}$, R_{wavy}, and R_{in}, which were calculated from the calling times of the 6 male Japanese tree frogs. Red, blue, green, and black lines represent the time series data of $R_{cluster}$, R_{wavy} for $k = 1$ and $k = -1$, and R_{in}, respectively. $R_{cluster}$ stably took considerably larger values than R_{wavy} and R_{in}, which meant that two-cluster antisynchronization was realized in this chorus.

this analysis, 50% of the maximum light intensity of respective devices was used as a threshold value.

Figure 7B shows the calling times of 6 frogs obtained from the light pattern shown in Figure 7A. We observed that some pairs called synchronously. For instance, the 2nd and 3rd frogs stably synchronized in almost anti-phase. The calling times of the nth frog were then described by t_n^j, where j represented the jth calling, and the phase of the nth frog at time t was evaluated as follows[6,9]:

$$\theta_n = 2\pi \frac{t - t_n^j}{t_n^{j+1} - t_n^j}, \qquad (4)$$

where t_n^j and t_n^{j+1} described the times of the two calls covering time t. We did not calculate the phase in the case of $t_n^{j+1} - t_n^j > 1.0$ or $t_n^{j+1} - t_n^j < 0.2$, because the inter-call intervals of a single Japanese tree frog were around 0.25 sec[5]. Subsequently, the order parameters $R_{cluster}$, R_{wavy} and R_{in} were estimated during the collective choruses of more than 3 frogs, by substituting the time series data of θ_n to equations (1) and (2) and to $R_{in} = \left| \sum_{n=1}^{N} \exp(i\theta_n) \right| / N$[8]. Figure 7C represents the time series data of $R_{cluster}$, R_{wavy} and R_{in}. It was shown that $R_{cluster}$ stably took considerably larger values than R_{wavy} and R_{in}, which meant that two-cluster antisynchronization was realized in this chorus of the 6 male frogs. In addition to the data shown in Figure 7 that were recorded on 15th June in 2011, we analyzed the data recorded on 12th, 14th, 16th, and 17th June in 2011, and calculated the order parameters of $R_{cluster}$, R_{wavy} and R_{in}. It should be noted that we did not analyze the data recorded on 11th June in 2011 (see Methods), since the data were too complicated to precisely estimate the positions of calling frogs because of the presence of a very large number of calling frogs (Fig.S7 in Supplementary information).

To examine the reproducibility of two-cluster antisynchronization, we performed two kinds of analyses. First, the mean values of the order parameters were calculated as $\bar{R}_{cluster}$, $\bar{R}_{wavy}$ for $k = 1$ and -1, and $\bar{R}_{in}$, from the 15 min video data of the 5 field observations (Table 1A). It was shown that $\bar{R}_{cluster}$ was larger than $\bar{R}_{wavy}$ for $k = 1$ and -1, and $\bar{R}_{in}$ in all the data. Second, the ratio of each state was calculated from the same data (Table 1B), by estimating the total duration when the order parameters exceeded a threshold value of 0.8. This analysis demonstrated that the ratio of two-cluster antisynchronization was considerably larger than the ratios of the other states. Thus, two-cluster antisynchronization of male Japanese tree frogs was more frequently observed at an actual paddy field.

Discussion

This paper presents theoretical and experimental studies on spatio-temporal dynamics in collective frog choruses. First, a mathematical model is proposed to describe the nonlinear dynamics inherent in the calling times and positions of male Japanese tree frogs. The numerical simulation shows that organized spatio-temporal dynamics, i.e., two-cluster antisynchronization and wavy antisynchronization, are realized in the mathematical model (Figs. 2 and 3). Second, the stability of two-cluster and wavy antisynchronization is analyzed by numerically varying the length parameters of a rectangular paddy field. It is demonstrated that two-cluster antisynchronization is more frequently observed than wavy antisynchronization (Fig. 4B). Finally, field research was performed on actual choruses of male Japanese tree frogs at a paddy field by using our sound-imaging method[14]. Analysis of the recorded video showed that two-cluster antisynchronization was more frequently detected in choruses of male Japanese tree frogs (Fig. 7 and Table 1). Thus, the present mathematical model qualitatively explains the result of the field research, i.e., the existence of two-cluster antisynchronization in the choruses of male Japanese tree frogs.

As for the spatial structures in frog choruses, our field research revealed that calling frogs were sparsely positioned along an edge of a paddy field at an interval ranging from 0.8 to 3.2 m (Fig. 7B), using the spatial resolution by the devices deployed at intervals of 40 cm. In general, most frog species can be classified as either explosive or prolonged breeders[2,15]. Experimental studies have shown that, whereas explosive breeders exhibit considerably denser distribution in their breeding site, prolonged breeders exhibit sparser distribution[2,15]. Since Japanese tree frogs are classified as prolonged breeders[4,15], their sparse spatial distribution revealed by our field research can be well understood on the basis of their breeding type. Moreover, as shown in Figures 2A, 3A, and 5A, our mathematical model qualitatively explains the sparse distribution of male Japanese tree frogs according to the competitive interaction terms described by equations (7) and (8).

As for the spatio-temporal dynamics in frog choruses, wavy antisynchronization was rarely detected in the field research, although it appeared as a stable solution in the numerical simulation (see Figs. 3 and 4B). This inconsistency may be explained by a specific field condition observed during our recordings. At the paddy field shown in Figure 6C, the sound-imaging devices were deployed along one edge of the field where a considerably larger number of male frogs aggregated than along the other 3 edges of the field (see Methods). Therefore, the calling frogs mainly aligned along the one edge covered by our recording system, and then straight-line distribution of

Table 1 | Stability analyses of synchronization states on the basis of the 5 field observations. In this table, Data (1)–(5) correspond to the 15 min video data recorded on 12th, 14th, 15th, 16th, and 17th June in 2011, respectively. Note that we did not use the data recorded on 11th June in 2011, since the data were too complicated to precisely estimate the positions of calling frogs because of the presence of a very large number of calling frogs at the paddy field (Fig.S7 in Supplementary information). (A) The averaged order parameters of two-cluster antisynchronization, in-phase synchronization, and wavy antisynchronization. The total duration of choruses including more than 3 frogs were 11.5 min, 1.7 min, 5.2 min, 0.9 min, and 12.34 min, respectively. By using these data sets of the choruses, we estimated the mean values of the order parameters as $\bar{R}_{cluster}$, $\bar{R}_{in}$, and $\bar{R}_{wavy}$. It was shown that $\bar{R}_{cluster}$ was larger than $\bar{R}_{wavy}$ for $k = 1$ and -1, and $\bar{R}_{in}$ in all the field observations. (B) Ratios of two-cluster antisynchronization, in-phase synchronization, and wavy antisynchronization. In this analysis, we summed up the times when each order parameter exceeded a threshold value of 0.8, and then divided the duration of each state by the total chorus duration of more than 3 frogs. The ratio of two-cluster antisynchronization was considerably larger than those of in-phase synchronization and wavy antisynchronization

A

	$\bar{R}_{cluster}$	$\bar{R}_{in}$	$\bar{R}_{wavy}$ for k = 1	$\bar{R}_{wavy}$ for k = −1
Data (1)	0.432	0.358	0.336	0.324
Data (2)	0.567	0.414	0.348	0.348
Data (3)	0.550	0.343	0.350	0.345
Data (4)	0.573	0.336	0.356	0.356
Data (5)	0.484	0.368	0.305	0.312

B

	Two-cluster antisync	Insync	Wavy antisync for $k = 1$	Wavy antisync for $k = -1$
Data (1)	4.48%	1.84%	0.85%	0.76%
Data (2)	19.88%	9.03%	1.09%	1.19%
Data (3)	17.70%	1.36%	2.00%	2.01%
Data (4)	23.64%	1.39%	2.46%	2.46%
Data (5)	7.87%	2.90%	0.25%	0.32%

the male frogs was approximately realized at the paddy field. Our numerical simulation suggests that, in such straight-line distribution of the male frogs, wavy antisynchronization is not observed, and only two-cluster antisynchronization is observed (see the case of (L_x, L_y) = (60, 0) in Fig. 4B). Furthermore, linear stability analysis has shown that two-cluster antisynchronization is asymptotically stable for the straight-line distribution (Fig.S2C in Supplementary information).

From the mathematical point of view, it is an important future problem to examine the stability of two-cluster and wavy antisynchronization by varying the parameter values in the present mathematical model. In particular, we expect that the stability can be affected by the number of the male frogs, N, which is fixed as $N = 20$ in this study. For example, exact two-cluster antisynchronization cannot exist for circular distribution with odd values of N, because of frustration that all the neighboring pairs cannot synchronize in anti-phase[7]. In contrast, two-cluster antisynchronization for the straight-line distribution can remain as a stable equilibrium state even for odd values of N, because all the neighboring pairs along the straight line can synchronize in anti-phase as $\theta_n - \theta_{n+1} = \pi$ (mod 2π), for $n = 1, 2, …, N - 1$.

As shown in Figure 7C, the order parameters $R_{cluster}$, R_{wavy} and R_{in} showed complex dynamics during the recording at the paddy field.

This result suggests that male Japanese tree frogs dynamically change their calling times even in the same chorus beyond the expectation of the present mathematical model. Further studies are required to derive a mathematical model explaining such complex dynamics observed in an actual field. For the modification of the present mathematical model, it is useful to estimate three functions, $\Gamma_{nm}(\theta_m - \theta_n, r_m - r_n)$, $F_{nm}(\theta_m - \theta_n, r_m - r_n)$, and $G_n(r_n)$, on the basis of laboratory experiments and field research. The functions $\Gamma_{nm}(\theta_m - \theta_n, r_m - r_n)$ and $F_{nm}(\theta_m - \theta_n, r_m - r_n)$ may be estimated by laboratory experiments. For instance, recording of two calling frogs that hop around a room can be used to represent fundamental data to study the interactions between two individuals. Subsequently, $\Gamma_{nm}(\theta_m - \theta_n, r_m - r_n)$ may be estimated according to the method provided in the reference 16 that makes it possible to calculate the interaction terms in the phase oscillator model from the desynchronized time series data of two interacting elements. However, it seems to be difficult to experimentally determine $G_n(r_n)$, because male Japanese tree frogs move to a paddy field without emitting calls according to our field observations. A sound-imaging method cannot be applied to such silent frogs, and other tracking methods need to be developed.

Advertisement calls of male frogs have two roles, i.e., attracting conspecific females and defending their own territories[2]. In this section, the behavioral meanings of two-cluster antisynchronization are discussed based on these two roles of advertisement calls. As regards the first role of attracting conspecific females, two-cluster antisynchronization of male frogs can strengthen the sound-pressure level of their chorus, because male frogs involved in the same cluster call synchronously almost in-phase. Such a collective chorus with a high sound-pressure level may attract more females far from the chorus site. After the females arrive at the breeding site, the males must compete against each other to mate with one of the females. In this final step, the calling properties of individual male frogs, e.g., sound-pressure level and frequency, can be also important for attracting females[2], because such calling properties can include information about body sizes and physical conditions of the male frogs. As regards the second role of defending their territories, Figure 7B has demonstrated that neighboring pairs of male frogs, e.g., the pair of the 2nd and 3rd frogs and the pair of the 5th and 6th frogs, tend to call alternately in anti-phase. Such antisynchronization between neighboring males can help them to claim their own territories each other because of a small amount of call overlap[5,6,17]. If neighboring pairs of male frogs synchronize in anti-phase respectively, two-cluster antisynchronization is automatically realized. Therefore, antisynchronization of neighboring pairs can be the origin of global two-cluster antisynchronization. However, in-phase synchronization between a neighboring pair was also detected. For example, the pair of the 1st and 2nd frogs synchronized almost in-phase (Fig. 7B). The role of such cooperative behavior is still unknown and needs to be further examined.

The present mathematical model can be applied to theoretical studies on the collective behavior of other species of animals. For instance, several species of insects, such as fireflies, crickets and cicadas, interact with each other by periodically emitting signals involving lights and sounds[9]. The nonlinear dynamics in the collective behavior of such animals can be examined on the basis of our mathematical model, by varying the interaction terms $\Gamma_{nm}(\theta_m - \theta_n, r_m - r_n)$ and $F_{nm}(\theta_m - \theta_n, r_m - r_n)$, and the geometric shape of their habitats. In addition, when the target animals are nocturnal and interact through sounds, our sound-imaging method can be similarly applied to detect their calling times and positions[14]. However, it should be noted that the present method has several limitations. One of the limitations is that we had to manually tune the gain of each *Firefly*[14], and then the response of each *Firefly* to the same sound could have been slightly different. Such a difference in the tuning can cause the problem that the position of a single frog is detected twice.

For example, in the data of Figure S4 shown in Supplementary information, two close peaks at the 31st and 33rd devices were detected as the positions of calling frogs, respectively. In addition, the calling times estimated from the light patterns of the two devices were almost the same. We speculate that these signals of the 31st and 33rd devices originated from the calls of a single frog, since the 32nd device weakly responded to the calls because of bad device tuning. In this study, we carefully chose suitable threshold values in the data analysis to avoid this problem. However, further studies to improve the device performance and data analysis method are required.

Methods

Mathematical modeling of collective frog choruses. To theoretically examine the spatio-temporal structures realized in the choruses of male Japanese tree frogs, we propose a mathematical model describing their behavior in an actual field. Whereas a single male Japanese tree frog calls periodically, a pair of the male frogs interact through sounds[5,6]. In addition, the male frogs hop around fields in natural habitats. We model such dynamics in calling times and positions of the male frogs originating from their acoustic interactions, as follows (Fig. 1):

$$\frac{d\theta_n}{dt} = \omega_n + \sum_{m=1, m \neq n}^{N} \Gamma_{nm}(\theta_m - \theta_n, \boldsymbol{r}_m - \boldsymbol{r}_n), \quad (5)$$

$$\frac{d\boldsymbol{r}_n}{dt} = \sum_{m=1, m \neq n}^{N} \boldsymbol{F}_{nm}(\theta_m - \theta_n, \boldsymbol{r}_m - \boldsymbol{r}_n) + \boldsymbol{G}_n(\boldsymbol{r}_n), \quad (6)$$

where θ_n ($n = 1, 2, \ldots, N$) represents the phase of the calling of the nth frog[5-7], and the vector $\boldsymbol{r}_n$ represents the position of the nth frog in a two-dimensional space. The parameter ω_n represents the angular velocity of the calling of the nth frog. It is then assumed that $\theta_n = 0 \pmod{2\pi}$ corresponds to the timing of the calls emitted by the nth frog, so as to explain the periodic calling behavior of the isolated male frogs[5,6]. The functions $\Gamma_{nm}(\theta_m - \theta_n, \boldsymbol{r}_m - \boldsymbol{r}_n)$ and $\boldsymbol{F}_{nm}(\theta_m - \theta_n, \boldsymbol{r}_m - \boldsymbol{r}_n)$ ($n, m = 1, 2, \ldots, N$ and $n \neq m$) represent the effects from the mth frog to the nth frog. By simply extending the phase oscillator model described by $d\theta_n/dt = \omega_n + \sum_{m=1, m \neq n}^{N} \Gamma_{nm}(\theta_m - \theta_n)$[8], $\Gamma_{nm}(\theta_m - \theta_n, \boldsymbol{r}_m - \boldsymbol{r}_n)$ and $\boldsymbol{F}_{nm}(\theta_m - \theta_n, \boldsymbol{r}_m - \boldsymbol{r}_n)$ are defined as 2π-periodic functions of the phase difference, $\theta_m - \theta_n$, and also functions of the relative position between the nth and mth frogs, $\boldsymbol{r}_m - \boldsymbol{r}_n$. The function $\boldsymbol{G}_n(\boldsymbol{r}_n)$ is used to explain our field observations that male Japanese tree frogs aggregate along the edges of paddy fields in natural habitats[14]. Moreover, the geometric shape of the field is first assumed to be a circle, for simplicity; the radius of the field is described by the positive constant L, and the center of the field is set at the origin $\boldsymbol{0}$ in the two-dimensional space (Fig. 1).

Then, we determine the three functions $\Gamma_{nm}(\theta_m - \theta_n, \boldsymbol{r}_m - \boldsymbol{r}_n)$, $\boldsymbol{F}_{nm}(\theta_m - \theta_n, \boldsymbol{r}_m - \boldsymbol{r}_n)$, and $\boldsymbol{G}_n(\boldsymbol{r}_n)$ in equations (5) and (6), based on experimental results and field observations of the behavior of male Japanese tree frogs.

Laboratory experiments revealed that two individuals of male Japanese tree frogs, which were placed in small cages respectively, called alternately almost in anti-phase π[5,6]. To qualitatively explain this antisynchronization (or call alternation) unique to male Japanese tree frogs, we used the phase oscillator model with a simple sinusoidal function[7], i.e., $d\theta_n/dt = \omega_n - \sum_{m=1, m \neq n}^{N} K_{nm} \sin(\theta_m - \theta_n)$. By extending the model, we define $\Gamma_{nm}(\theta_m - \theta_n, \boldsymbol{r}_m - \boldsymbol{r}_n)$ in equation (5) as follows:

$$\Gamma_{nm}(\theta_m - \theta_n, \boldsymbol{r}_m - \boldsymbol{r}_n) = -\frac{K_{nm}}{|\boldsymbol{r}_m - \boldsymbol{r}_n|^2} \sin(\theta_m - \theta_n). \quad (7)$$

Because the male frogs interact through sounds that decay proportional to the inverse of the square of their distance, $\Gamma_{nm}(\theta_m - \theta_n, \boldsymbol{r}_m - \boldsymbol{r}_n)$ is assumed to be a function of $1/|\boldsymbol{r}_m - \boldsymbol{r}_n|^2$. The parameter K_{nm} represents a positive symmetrical coupling coefficient between the nth and mth frogs, i.e., $K_{nm} = K_{mn}$.

The calling behavior of male Japanese tree frogs studied here is classified as advertisement calls. In general, advertisement calls of male frogs have two roles of attracting conspecific females and also claiming their own territories to other conspecific males[2]. The important point is that, during antisynchronization of two individuals, information included in calls of one individual is not masked by calls of the other individual because of a small amount of call overlap[17]. These two properties of advertisement calls suggest that antisynchronization is capable of helping each pair of male frogs to mutually interact and then robustly defend their own territories[5,6]. To model this conjecture about antisynchronization, $\boldsymbol{F}_{nm}(\theta_m - \theta_n, \boldsymbol{r}_m - \boldsymbol{r}_n)$ in equation (6) is defined as follows:

$$\boldsymbol{F}_{nm}(\theta_m - \theta_n, \boldsymbol{r}_m - \boldsymbol{r}_n) = \frac{K_{nm}}{|\boldsymbol{r}_m - \boldsymbol{r}_n|^2} (1 - \cos(\theta_m - \theta_n)) \boldsymbol{e}_{nm}. \quad (8)$$

Here, $\boldsymbol{F}_{nm}(\theta_m - \theta_n, \boldsymbol{r}_m - \boldsymbol{r}_n)$ is assumed to include the factor $K_{nm}/|\boldsymbol{r}_m - \boldsymbol{r}_n|^2$ as in the case of $\Gamma_{nm}(\theta_m - \theta_n, \boldsymbol{r}_m - \boldsymbol{r}_n)$, because $\boldsymbol{F}_{nm}(\theta_m - \theta_n, \boldsymbol{r}_m - \boldsymbol{r}_n)$ also models the interaction of the male frogs via calling sounds. Moreover, $\boldsymbol{F}_{nm}(\theta_m - \theta_n, \boldsymbol{r}_m - \boldsymbol{r}_n)$ is assumed to include the factor $(1 - \cos(\theta_m - \theta_n)) \boldsymbol{e}_{nm}$, where $\boldsymbol{e}_{nm}$ is a unit vector between $\boldsymbol{r}_n$ and $\boldsymbol{r}_m$, i.e., $\boldsymbol{e}_{nm} = -\frac{\boldsymbol{r}_m - \boldsymbol{r}_n}{|\boldsymbol{r}_m - \boldsymbol{r}_n|}$. In this term, $1 - \cos(\theta_m - \theta_n)$ takes the

maximum positive value at $\theta_m - \theta_n = \pi$, which means that the nth and mth frogs attempt to move towards the opposite directions during antisynchronization; $1 - \cos(\theta_m - \theta_n)$ takes the minimum value of 0 at $\theta_m - \theta_n = 0$, which means that the nth and mth frogs do not affect their positions each other during in-phase synchronization. It should be noted that male frogs face difficulties in their acoustic interaction during in-phase synchronization because of a large amount of call overlap.

We previously observed that male Japanese tree frogs aggregated along the edges of paddy fields[14]. To explain such localized spatial distribution of male Japanese tree frogs, $\boldsymbol{G}_n(\boldsymbol{r}_n)$ is defined as follows:

$$\boldsymbol{G}_n(\boldsymbol{r}_n) = (L - |\boldsymbol{r}_n|) \boldsymbol{e}_n, \quad (9)$$

where $\boldsymbol{e}_n$ represents a unit vector between the position of the nth frog $\boldsymbol{r}_n$ and the center of the paddy field $\boldsymbol{0}$, i.e., $\boldsymbol{e}_n = \frac{\boldsymbol{r}_n}{|\boldsymbol{r}_n|}$. Furthermore, $\boldsymbol{G}_n(\boldsymbol{r}_n)$ is assumed to include the factor $L - |\boldsymbol{r}_n|$. Here, $L - |\boldsymbol{r}_n|$ is negative when the nth frog is positioned outside the circular paddy field, and then the frog is attracted to the edge of the field; on the other hand, $L - |\boldsymbol{r}_n|$ is positive when the nth frog is positioned inside the circular paddy field, and the frog is attracted to the edge of the field as well. Equation (3) of $\boldsymbol{G}_n(\boldsymbol{r}_n) = \boldsymbol{r}_n^* - \boldsymbol{r}_n$ is used instead of equation (9) for a rectangular paddy field.

Recording of frog choruses at an actual paddy field. To test the hypothesis of our numerical simulation suggesting that two-cluster antisynchronization can be frequently observed in the choruses of male Japanese tree frogs (Fig. 4B), the positions and calling times of individual frogs must be obtained. For this purpose, we used a sound-imaging method[14]. The imaging method is based on the device named *Firefly* consisting of a microphone and a light emitting diode (LED)[14] (Fig. 6B); the LED of the *Firefly* unit is illuminated, when capturing nearby sounds. Along one edge of a paddy field where a considerably larger number of male Japanese tree frogs were calling than along the other three edges, 85 or 86 devices were deployed at intervals of 40 cm (Fig. 6C); the illumination pattern of the devices was recorded by a Sony video camera (HDR- XR550V, 29.97 fps). Note that the lights of some devices were not detected, when those devices were deployed far from the camera and were not illuminated by frog calls. We carefully checked all the data, and confirmed that the lights of at least 40 devices close to the camera were stably captured even when those devices were not strongly illuminated by frog calls. Hence, we used the light patterns of 40 devices close to the camera for data analysis. An index was attached to each device from one end of the edge, which was closer to the camera, to the other end.

Recordings were carried out between 20:00 h and 24:00 h on 11th, 12th, 14th, 15th, 16th, and 17th June, 2011, in Oki island, Shimane, Japan. The ambient temperature ranged between 15°C and 21.5°C, and the humidity ranged between 49% and 93%. The data corresponding to the first 15 min of all the recorded video were then divided into dozens of pictures. All the field observations in this study were performed in accordance with the guidelines approved by the Wako Animal Experiments Committee of RIKEN and the Animal Experimental Committee of Kyoto University.

1. Gerhardt, H. C. & Huber, F. *Acoustic Communication in Insects and Anurans*, (University of Chicago Press, Chicago, 2002).
2. Wells, K. D. *The Ecology and Behavior of Amphibians*, (The University of Chicago Press, Chicago, 2007).
3. Narins, P. M. *et al. Hearing and Sound Communication in Amphibians*, (Springer Science + Business Media, New York, 2007).
4. Maeda, N. & Matsui, M. *Frogs and Toads of Japan*, (Bun-ichi Sogo Shuppan Co. Ltd., Tokyo, 1999).
5. Aihara, I. Modeling synchronized calling behavior of Japanese tree frogs. *Phys. Rev. E* **80**, 011918 (2009).
6. Aihara, I. *et al.* Complex and transitive synchronization in a frustrated system of calling frogs. *Phys. Rev. E* **83**, 031913 (2011).
7. Aihara, I. & Tsumoto, K. Nonlinear dynamics and bifurcations of a coupled oscillator model for calling behavior of Japanese tree frogs (*Hyla japonica*). *Math. Biosci.* **214**, 6–10 (2008).
8. Kuramoto, Y. *Chemical Oscillations, Waves, and Turbulence*, (Springer-Verlag, Berlin, 1984).
9. Pikovsky, A., Rosenblum, M. & Kurths, J. *Synchronization: A Universal Concept in Nonlinear Sciences*, (Cambridge University Press, Cambridge, 2001).
10. Sumino, Y. *et al.* Large-scale vortex lattice emerging from collectively moving microtubules. *Nature* **483**, 448–452 (2012).
11. Tanaka, D. General chemotactic model of oscillators. *Phys. Rev. Lett.* **99**, 134103 (2007).
12. Fujiwara, N., Kurths, J. & Guilera, A. D. Synchronization in networks of mobile oscillators. *Phys. Rev. E* **83**, 025101 (2011).
13. Aoki, T. & Aoyagi, T. Scale-free structures emerging from co-evolution of a network and the distribution of a diffusive resource on it. *Phys. Rev. Lett.* **109**, 208702 (2012).
14. Mizumoto, T. *et al.* Sound imaging of nocturnal animal calls in their natural habitat. *J. Comp. Physiol. A* **197**, 915–921 (2011).
15. Matsui, M. *Natural History of the Amphibia*, (University of Tokyo Press, Tokyo, 1996).
16. Miyazaki, J. & Kinoshita, S. Determination of a coupling function in multicoupled oscillators. *Phys. Rev. Lett.* **96**, 194101 (2006).

17. Yoshida, S. & Okanoya, K. Evolution of turn-taking: A bio-cognitive perspective. *Cogn. Studies* **12**, 153–165 (2005).

Author contributions

I.A. produced the original idea of the mathematical model and performed the numerical simulation. I.A., T.M., T.O., H.A. and K.N. conducted field research. I.A. analyzed the data of the field research. I.A., T.M., T.O., H.A., K.N., H.G.O. and K.A. wrote and revised the paper.

Additional information

Supplementary information accompanies this paper at http://www.nature.com/scientificreports

Competing financial interests: The authors declare no competing financial interests.

How to cite this article: Aihara, I. *et al.* Spatio-Temporal Dynamics in Collective Frog Choruses Examined by Mathematical Modeling and Field Observations. *Sci. Rep.* **4**, 3891; DOI:10.1038/srep03891 (2014).